Anomaly effects of orthogonal paired-arrays for 3D geoelectrical resistivity imaging

A. P. Aizebeokhai & A. I. Olayinka

Environmental Earth Sciences

ISSN 1866-6280
Volume 64
Number 8

Environ Earth Sci (2011) 64:2141-2149
DOI 10.1007/s12665-011-1041-9

Springer

Environ Earth Sci (2011) 64:2141–2149
DOI 10.1007/s12665-011-1041-9

ORIGINAL ARTICLE

Anomaly effects of orthogonal paired-arrays for 3D geoelectrical resistivity imaging

A. P. Aizebeokhai · A. I. Olayinka

Received: 1 February 2010 / Accepted: 19 March 2011 / Published online: 1 April 2011

Abstract A series of 2D apparent resistivity data were generated over two synthetic models representing different geological or environmental conditions commonly associated with geophysical applications for hydrogeological, environmental and engineering investigations. The apparent resistivity data were generated for the following arrays: Wenner-alpha (WA), Wenner-beta (WB), Wenner–Schlumberger (WSC), dipole–dipole (DDP), pole–dipole (PDP) and pole–pole (PP) arrays, which were paired such that apparent resistivity data for 2D profiles in a parallel direction are obtained with a particular array type and those in a perpendicular direction are observed with a different array type. The 2D apparent resistivity data for the orthogonal paired-arrays were then collated to 3D data sets. The effectiveness and efficiency of the orthogonal paired-arrays in 3D geoelectrical resistivity imaging were evaluated by determining the mean absolute anomaly effects of the electrode configurations on the synthetic models. The results show that DDP–PDP, DDP–PP, DDP–WSC, PDP–PP, DDP–WB, PDP–WB and WB–WSC orthogonal paired-arrays produced higher anomaly effects on the synthetic models. This indicates that DDP–PDP, DDP–PP, DDP–WSC, PDP–PP, DDP–WB, PDP–WB and WB–WSC orthogonal paired-arrays are more sensitive to 3D features of the geologic models than the other orthogonal paired-arrays investigated.

A. P. Aizebeokhai (✉)
Department of Physics, Covenant University, Ota, Nigeria
e-mail: philips_a_aizebeokhai@yahoo.co.uk

A. I. Olayinka
Department of Geology, University of Ibadan, Ibadan, Nigeria
e-mail: aiolayinka@yahoo.com

Keywords Orthogonal paired-arrays · 3D surveys · Geoelectrical · Resistivity imaging · Anomaly effects · Measurement effectiveness

Introduction

Geoelectrical resistivity imaging has played an important role in addressing a wide variety of hydrological, environmental and geotechnical issues. In most geophysical applications to environmental and engineering investigations, the geology is usually complex, subtle and multi-scale such that both lateral and vertical variations of the subsurface petrophysical properties can be very rapid and erratic. Two-dimensional (2D) geoelectrical resistivity imaging, in which the subsurface resistivity is assumed to vary both laterally and vertically along the survey line but constant in the perpendicular direction, has been widely used to map areas with moderately complex geology (e.g. Griffiths et al. 1990; Griffiths and Barker 1993; Dahlin and Loke 1998; Olayinka 1999; Olayinka and Yaramanci 1999; Amidu and Olayinka 2006; Aizebeokhai et al. 2010). However, geological structures and subsurface petrophysical properties are inherently three-dimensional (3D) and the 2D assumption is commonly violated; this often leads to out-of-plane resistivity anomaly in the 2D images which could be misleading in the interpretation of subsurface features (Bentley and Gharibi 2004). Thus, a 3D geoelectrical resistivity imaging which allows resistivity variation in all possible directions should give a more accurate and reliable image of the subsurface, especially in highly heterogeneous subsurface commonly associated with environmental, hydrological and engineering investigation sites.

What constitutes a 3D data set that would yield significant 3D subsurface information for geoelectrical

resistivity imaging is not clearly understood. Ideally, a 3D geoelectrical resistivity survey is one in which the measurements of apparent resistivity values are made in all possible directions. The techniques for conducting 3D electrical resistivity imaging have been presented by Loke and Barker (1996). The use of pole–pole (PP; e.g. Li and Oldenburg 1994; Loke and Barker 1996; Park 1998) and pole–dipole (PDP; e.g. Chambers et al. 1999; Ogilvy et al. 1999) arrays in 3D electrical resistivity imaging surveys have been reported in literature. Square and rectangular grids with constant electrode spacing in both *x*- and *y*-directions, in which each electrode is in turn used as current electrode and the potential measured at all other electrodes, were commonly used. But these methods which allow the measurements of complete 3D data sets are in most cases impractical because of the length of cables, the number of electrodes, site geometry and electrode spacing involved in practical surveys. In addition, the measurement of 3D complete data sets using the square or rectangular grid is time consuming and cumbersome in surveys involving large grids since the number of possible electrode permutations for the measurements will be very large.

To reduce the number of data measurements and the time and effort required for 3D geoelectrical resistivity field surveys, a cross-diagonal surveying method in which potential measurements are only made at the electrodes along the *x*-axis, *y*-axis and 45° diagonal lines was proposed by Loke and Barker (1996). The number of possible independent measurement for the cross-diagonal surveying method will still be very large for medium to large grid of electrodes and thus time consuming to acquire, especially if a single channel or a manual data acquisition system is employed. In contrast to the cross-diagonal surveying method, sets of parallel 2D lines (e.g. Chambers et al. 2002; Bentley and Gharibi 2004) and orthogonal 2D lines (e.g. Aizebeokhai et al. 2009, 2010) which allow flexible survey design, choice of array and easy adaptability to data acquisition systems have been used to construct 3D images. Most of the 3D geoelectrical resistivity surveys that have been conducted indicate that the 3D images produced from the 3D inversions are superior to 2D images and the quasi-3D images produced from 2D inversions.

Traditionally, the imaging capability and efficiency of different electrode configurations differ for different geological structures. The effectiveness and imaging capabilities of geoelectrical resistivity measurements for a given configuration of electrodes can be evaluated using the anomaly effect (Militzer et al. 1979; Dahlin and Zhou 2004). For an effective geoelectrical resistivity survey, the value of the anomaly effect should be significantly greater than the background noise of the electrode configuration. Thus, anomaly effect is a measure of the signal-to-noise ratio of the electrode arrays and should vary with different geological models for a given electrode configuration. Geoelectrical resistivity measured data with high anomaly information usually produce good quality, high resolution and reliable inversion images. Field measurements are usually contaminated by different kinds of noise depending on the noise sensitivity to electrode configuration used for the measurements. The contamination of field observations with noise generally depends on the potential values measured, and hence the observed apparent resistivity data. The anomaly effects of electrode arrays can, therefore, be estimated using the measured apparent resistivity values. The apparent resistivity values allow us to qualitatively access the totality of the subsurface geological and petrophysical features with respect to the geometrical configurations of the electrodes used in observing the apparent resistivity data. Thus, the effectiveness and imaging capabilities of different electrode configurations can be suitably compared using the apparent resistivity data (and hence anomaly effect) obtained for the different electrode configurations over the same geological features.

The relative advantages of the arrays can be harnessed and maximised by combining apparent resistivity data sets of different arrays. In this paper, synthetic models were used to generate apparent resistivity data in a series of parallel and perpendicular 2D profiles of Wenner-alpha (WA), Wenner-beta (WB), Wenner–Schlumberger (WSC), dipole–dipole (DDP), PDP and PP. These arrays were paired in orthogonal form such that apparent resistivity data of 2D profiles in parallel direction are obtained using one array type and those of 2D profiles in a perpendicular direction are obtained with another array type. The series of 2D apparent resistivity data of the orthogonal paired-arrays generated over the synthetic models were collated to 3D data sets which were then processed using a full 3D inversion code (RES3DINV). The relative effectiveness and imaging capabilities of the orthogonal paired-arrays for 3D geoelectrical resistivity surveys were evaluated by determining the anomaly effects of these orthogonal paired-arrays on two synthetic models that simulate different geological conditions commonly associated with geophysical applications for hydrogeological, environmental and engineering investigations. The responses of these model structures to 3D geoelectrical resistivity surveying using a combination of 2D profiles for different orthogonal paired-arrays were assessed using the anomaly effect of the arrays on the synthetic models which is a measure of the signal-to-noise ratio of the surveys.

Basic theory of geoelectrical resistivity surveys

The goal of geoelectrical resistivity surveys is to determine the distribution of subsurface resistivity by taking

measurements of the potential difference on the ground surface or borehole. Typically, an electric current I is injected into the ground through two electrodes and the resulting potential $\Delta\Phi$ is measured between two other electrodes. The apparent resistivity ρ_a, which depends on the electrode configuration, is determined from these measurements. If the ground is homogeneous, the apparent resistivity equals the true resistivity. But for a typical heterogeneous subsurface, the true resistivity as a function of depth is estimated by inverting the measured apparent resistivity data set. Anomalous conditions or heterogeneities are then inferred from the inverse resistivity models. Low-frequency alternating current is employed as source signals in the DC resistivity surveys in determining subsurface resistivity distributions. Thus, the magnetic properties of the materials can be ignored (Telford et al. 1976) so that Maxwell's equations of electromagnetism reduced to:

$$\nabla \cdot \vec{E} = \frac{1}{\varepsilon_0} q, \tag{1}$$

$$\nabla \times \vec{E} = 0, \tag{2}$$

where $\vec{E}$ is the electric field in V/m, q is the charge density in C/m^3 and ε_0 is the permittivity of free space. These equations are applicable to continuous flow of direct current; however, they can be used to represent the effects of alternating currents at low frequencies such that the displacement currents and induction effects are negligible. Usually, a complete homogeneous and isotropic earth medium of uniform resistivity is assumed. For a continuous current flowing in an isotropic and homogeneous medium, the current density $\vec{J}$ is related to the electric field, $\vec{E}$ through Ohm's law $\vec{J} = \sigma\vec{E}$. The electric field vector $\vec{E}$ can be represented as the gradient of the electric scalar potential $\vec{E} = -\nabla\Phi$. This gives the fundamental Poisson equation for electrostatic fields as

$$\nabla^2\Phi(x, y, z) = -\frac{1}{\varepsilon_0} q(x, y, z). \tag{3}$$

The current sources in typical electrical resistivity surveys are usually point sources. Thus, the current and the current density over a volume element ΔV around a current source I located at (x_s, y_s, z_s) are given by the relation (Dey and Morrison 1979):

$$\nabla \cdot J = \left(\frac{I}{\Delta V}\right)\delta(x - x_s)\delta(y - y_s)\delta(z - z_s), \tag{4}$$

where δ is the Dirac delta function. Hence, the potential distribution due to a point current source is

$$-\nabla \cdot [\sigma(x,y,z)\nabla\Phi(x,y,z)] = \left(\frac{I}{\Delta V}\right)\delta(x-x_s)\delta(y-y_s)\delta(z-z_s). \tag{5}$$

This partial differential equation, which is a self-adjoint, strongly connected and non-separable elliptic equation of second order, gives the subsurface potential distribution in an isotropic non-uniform 3D medium due to a point current source. Numerous techniques have been developed to solve this problem, i.e. to determine the potential distribution that would be observed over a given subsurface structure. The potential $\Phi(x, y, z)$ and the normal component of the current density $\sigma\frac{\partial\Phi}{\partial n}$ are continuous across the boundary between two media of different resistivities but the current lines are refracted in accordance to the boundary conditions.

A number of electrode configurations have been used in recording geoelectrical resistivity survey data, each suitable for a particular geological situation. Regardless of the type of electrode array used, two procedures are adopted in classical resistivity surveys. The first is vertical electrical sounding (VES) (Koefoed 1979) where the centre point of the electrode array remains fixed, but the electrode spread is increased so as to obtain information of the variations in the subsurface resistivity with depth. The subsurface is assumed to consist of horizontal layers in which the resistivity varies only with depth but not laterally. Thus, the model of interpretation of VES is one-dimensional (1D) and is insensitive to lateral variations in the subsurface resistivity, which might lead to changes in apparent resistivity values. These changes are often misinterpreted as changes in resistivity with depth; however, useful results can be obtained for geological situations such as depth to bedrock and water table where the 1D model is approximately true. The second approach is the constant separation traversing (CST) or profiling where electrode separation remains fixed but the entire array is progressively moved along a straight line or profile. This yields information about lateral variations in the subsurface resistivity along the profile and is incapable of detecting variations with depth.

Two-dimensional geoelectrical resistivity surveys can be achieved by integrating the techniques of VES with that of electrical profiling. It involves apparent resistivity measurements from electrodes placed along a line using a range of different electrode separations and midpoints. The procedure is repeated for as many combinations of current and potential electrode positions as defined by the survey configuration. 2D resistivity imaging can be seen as a continuous vertical electrical sounding (CVES) in which a number of VES conducted in a grid are merged together or as a combination of successive profiles with increasing

electrode spacing. Two-dimensional resistivity surveys are usually carried out using large numbers of electrodes connected to multi-core cables. The 2D assumption is commonly violated because subsurface features are inherently 3D. Three-dimensional surveys are traditionally conducted using square or rectangular grid of electrodes. The development of automated data acquisition systems has significantly enhanced the efficiency and speed of measuring 2D and 3D data sets.

Description of the synthetic models

In order to investigate the capabilities of different electrode configurations in 3D geoelectrical resistivity imaging using a combination of orthogonal paired-arrays of 2D profiles, two synthetic model geometries representing different geological or environmental conditions were designed. The first is a 3D horst model structure that simulates a typical weathered or fractured profile in a crystalline basement complex in tropical areas (Aizebeokhai et al. 2009), while the other is a 3D trough model structure used to simulate the geological conditions of a typical waste dump site which is usually complex and subtle. The choice of these two geological conditions was informed because they are inherently associated with geophysical applications to hydrogeological, environmental and engineering investigations.

A 3D horst structure under an area of 100 × 100 m^2 (Fig. 1) with lateral variation in thickness such that the horst thickens towards the centre of the model where the least weathering is thought to occur and thinning outward with increasing weathering activities was assumed. The horst structure consists of a three-layer model comprising of the top soil, saprolite (the weathered zone) and the fresh basement. The top layer, corresponding to the top soil, was assigned a uniform thickness of 2.5 m and its resistivity varies laterally between 500, 700 and 400 Ω m from left to right. The weathered zone, represented with the thickness of the middle layer in the model structure, is thought to have undergone various lateral degrees of weathering or fracturing that increase outward. The thickness of the weathered zone is assumed to vary between a minimum of 5.75 m (depth 8.25 m) at the centre of the model structure where the least weathering occurs to a maximum of 13.50 m (depth 16.0 m) at the edges of the model considered to be most weathered. The weathered zone in crystalline basement complex is a product of chemical weathering which is usually a low resistive saprolite overlying a more resistive basement rocks (Carruthers and Smith 1992; Hazell et al. 1992). In addition, this zone is commonly aquiferous; thus, low resistivity model values varying between 150 and 100 Ω m were assigned to this layer. Underlying the weathered zone is a fresh basement of infinite thickness with a constant model resistivity value of 3,000 Ω m.

Similarly, the second synthetic model is a 3D trough structure also assumed to be under an area of 100 × 100 m^2 (Fig. 2), for convenience of electrode layouts. The synthetic trough model consists of three layers in which the thicknesses of the top and the middle layers vary

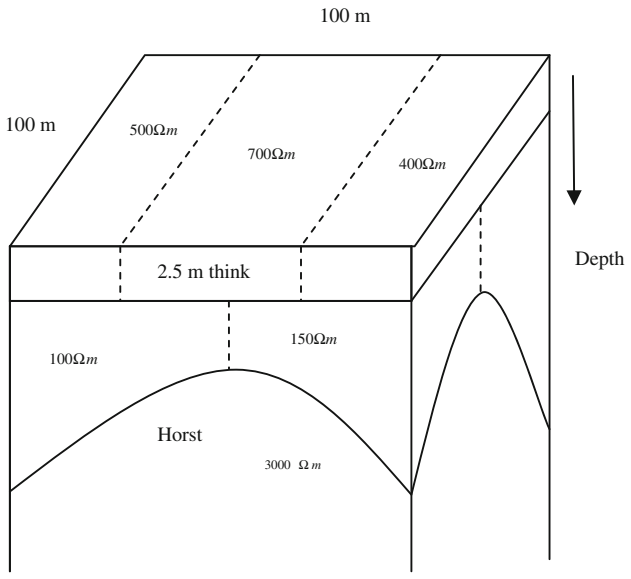

Fig. 1 A three-dimensional horst model simulating a typical weathered or fractured profile developed above crystalline basement complex

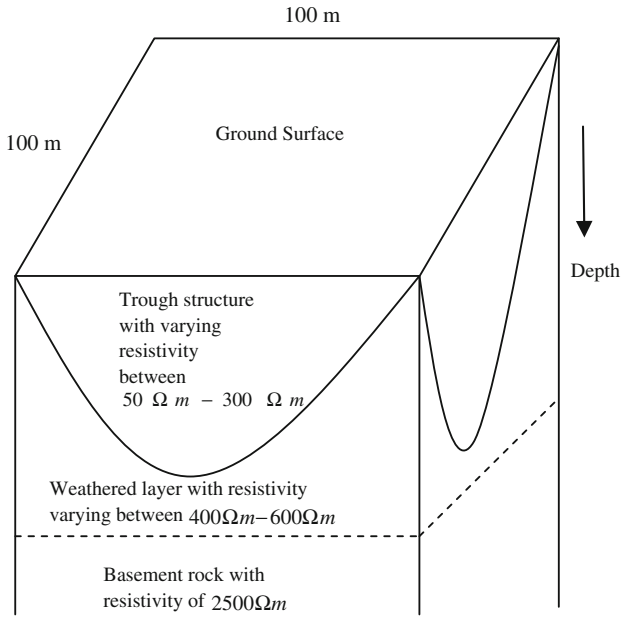

Fig. 2 A three-dimensional trough model simulating the geology of a waste dump site

with a maximum of 4.2 and 11.8 m, respectively, and the underlying third layer is a basement rock of infinite thickness. The trough structure is assumed to be at the centre of the model with varying lateral thickness and cutting across the first and second layers. Model resistivity values of 300 and 600 Ω m are assigned to the first and second layers, respectively, in their natural states. The trough structure and its surroundings are thought to be impacted by the deposited waste in the simulated dump site and hence would consist of laterally varying low resistivity values. Model resistivity values varying laterally between 50 and 250 Ω m, different from the assigned value of 300 and 600 Ω m in its natural state, were therefore assigned to the trough structure. Part of the second layer underlying the trough structure is also thought to be impacted by leachates from the deposited waste so that its model resistivity value varies to a minimum of 400 Ω m from the assigned value of 600 Ω m in its natural state. The leachates from the deposited waste in the simulated dump site are thought not to have reached the basement; thus, its resistivity would be approximately constant laterally. A constant model resistivity value of 2,500 Ω m was, therefore, assigned to the underlying basement of infinite thickness.

Determination of apparent resistivity and anomaly effects

The 3D synthetic model structures were approximated into series of 2D model structures separated with a constant interval in both parallel and perpendicular directions. Synthetic apparent resistivity data were calculated over the resulting orthogonal sets of 2D profiles using RES2DMOD forward modelling code for the selected arrays. The parallel 2D profiles which run in the east–west direction were denoted as in-lines while those in the perpendicular direction were denoted as cross-lines. Electrode layouts with different minimum separations a and inter-line spacing L ($a = 2$, 4, 5 and 10 m; $L = a$, $2a$, $2.5a$, $4a$, $5a$ and $10a$) were used in the calculation of the apparent resistivity data. The series of 2D model structures were subdivided into a number of homogeneous and isotropic blocks using a rectangular mesh. The mesh consists of four horizontal nodes per unit electrode spacing and the thickness increases with depth. The model resistivity value of each block in the mesh was supplied using an input text file. The 2D modelling accounts for 3D effect of current sources; thus, the resistivity of each of the models was allowed to vary arbitrarily along the profile and with depth, but with an infinite perpendicular extension.

The finite difference method (Dey and Morrison 1979), which basically determines the potentials at the nodes of the rectangular mesh, was employed in the calculation of the potential distribution. A double precision, which slightly takes a longer time but significantly more accurate, was used in the calculations of the potential distribution. The apparent resistivity values were normalised with the values of a homogeneous earth model so as to reduce the errors in the calculated potential values. The calculation errors are often less than 5%. The forward modelling grid used consists of four nodes per unit electrode. The calculated apparent resistivity values for each 2D profile for the different geological models were contaminated with 5% Gaussian noise (Press et al. 1996) so as to simulate field conditions.

In order to maximise the relative effectiveness and efficiency of the electrode arrays in geoelectrical resistivity imaging surveys, the electrode arrays used in calculating the apparent resistivity data were paired such that the 3D data sets were obtained by collating parallel 2D apparent resistivity data computed using one electrode array type with those in a perpendicular direction computed using a different electrode array. An orthogonal paired-array was thus formed for each 3D data set obtained. Apparent resistivity data for orthogonal 2D profiles for each of the arrays were also collated to 3D data. In addition, 3D apparent resistivity data were generated over the synthetic models for the arrays using RES3DMOD computer program which employs the conventional electrode square grids. This allows us to qualitatively compare, through anomaly effects of arrays on the models, the 3D apparent resistivity data obtained from the orthogonal paired-arrays to the 3D data sets obtained from the individual arrays using orthogonal 2D profiles. Similarly, the 3D data sets obtained using the conventional square or rectangular grids of electrodes were also compared with those of the orthogonal paired-array. The collation of the synthetic apparent resistivity data computed for the series of approximated 2D model structures to 3D data sets was done using RES2DINV inversion software (Loke and Barker 1996).

During the data collation, the coordinates, line direction, array type and electrode positions of each 2D profile were supplied to the computer program via a text file. The collations arranged the 2D apparent resistivity data and the electrode layouts in rectangular or square grid patterns according to the coordinates and direction of each 2D profile used, and electrode positions in the profile. Thus, the number of electrodes in each 2D profile, number of profiles collated and their directions determine the size and pattern of the electrode grid obtained. These parameters along with the data level attained for each array determine the data density of the resulting 3D data set. Since two different arrays were paired in orthogonal form, the computer code for the data collation assigned a general array to all data sets obtained using the orthogonal paired-arrays, as

the electrode arrangement for the orthogonal paired-arrays does not follow a particular order that can be recognised by the computer code. The 3D apparent resistivity values collated were then assessed with a full 3D inversion code (RES3DINV) and used to estimate the anomaly effects of the arrays and orthogonal paired-arrays on the synthetic models. The mean absolute anomaly effect on the models for a given electrode configuration was defined as:

$$\mathrm{AE} = \frac{\rho_{\max} - \rho_{\min}}{\rho_{\mathrm{av}}}, \tag{6}$$

where $\rho_{\max}$, $\rho_{\min}$ and ρ_{av} are maximum, minimum and average apparent resistivities, respectively, observed for the electrode configuration.

Results and discussion

The mean absolute anomaly effects of the selected electrode configurations on the synthetic models, using 3D data sets collated from orthogonal 2D profiles, are given in Figs. 3 and 4. The mean anomaly effects on the synthetic models for the various electrode grid sizes and inter-line spacing relative to the minimum electrode separation are presented. In general, electrode arrays with high anomaly effects on geological models usually produce better signal-to-noise ratio than electrode arrays with low anomaly effect. Consequently, arrays with high anomaly effects will yield inversion images with better resolution and model sensitivity than arrays with low anomaly effects. Anomaly effect of any electrode configuration varies from geological model to geological model depending on the resistivity contrast and the general background noise level. In Figs. 3 and 4, the anomaly effects of electrode arrays on the trough model are generally higher than the anomaly effect of electrode arrays on the horst model.

The anomaly effects presented in Figs. 3 and 4 generally show that DDP and PDP arrays yield larger anomaly effects on the horst model than the other arrays investigated. Similarly, DDP, PDP and WB arrays generally yield much larger anomaly effects on the trough model than any of the other arrays. In both synthetic models, WSC array generally yields moderate anomaly effect while the PP array gives the lowest anomaly effect. This result indicates that DDP and PDP arrays would be more sensitive to 3D features than the other arrays investigated and hence would produce better quality and higher resolution inversion models if the arrays are used for 3D surveys in which apparent resistivity data of orthogonal 2D profiles are collated. Reasonable and acceptable inversion models would be obtained if WSC array is used for the survey. On the other hand, PP array would yield the least model resolution and sensitivity; the observed low anomaly effect of the PP array could be due to the fact that PP array is more prone to picking telluric noise than any other array and the array has the deepest depth of penetration.

The observed anomaly effects for the orthogonal paired-arrays on the synthetic models are presented in Fig. 5.

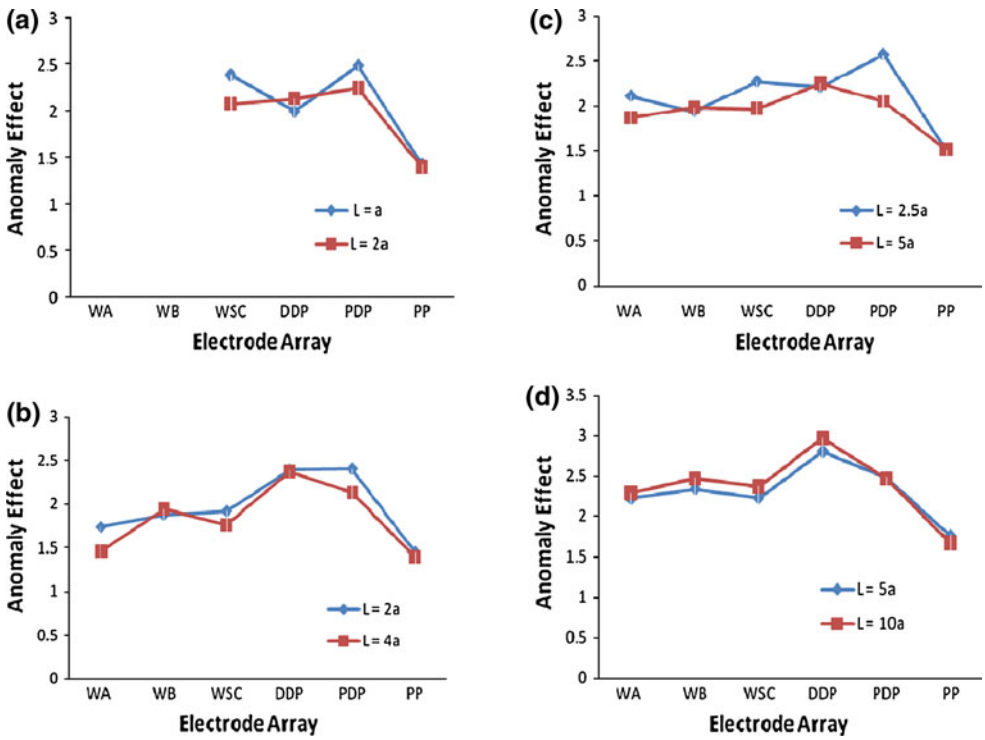

Fig. 3 Mean absolute anomaly effect of electrode arrays on the horst synthetic model. 3D geoelectrical resistivity imaging using orthogonal set of 2D profiles with grid size: **a** 11 × 11, **b** 21 × 21, **c** 26 × 26 ($L = 5a$) and 31 × 31 ($L = 2.5a$), and **d** 51 × 51; L is inter-line spacing and a is the minimum electrode separation. *WA* Wenner-alpha array, *WSC* Wenner–Schlumberger array, *PDP* pole–dipole array, *WB* Wenner-beta array, *DDP* dipole–dipole array, *PP* pole–pole array

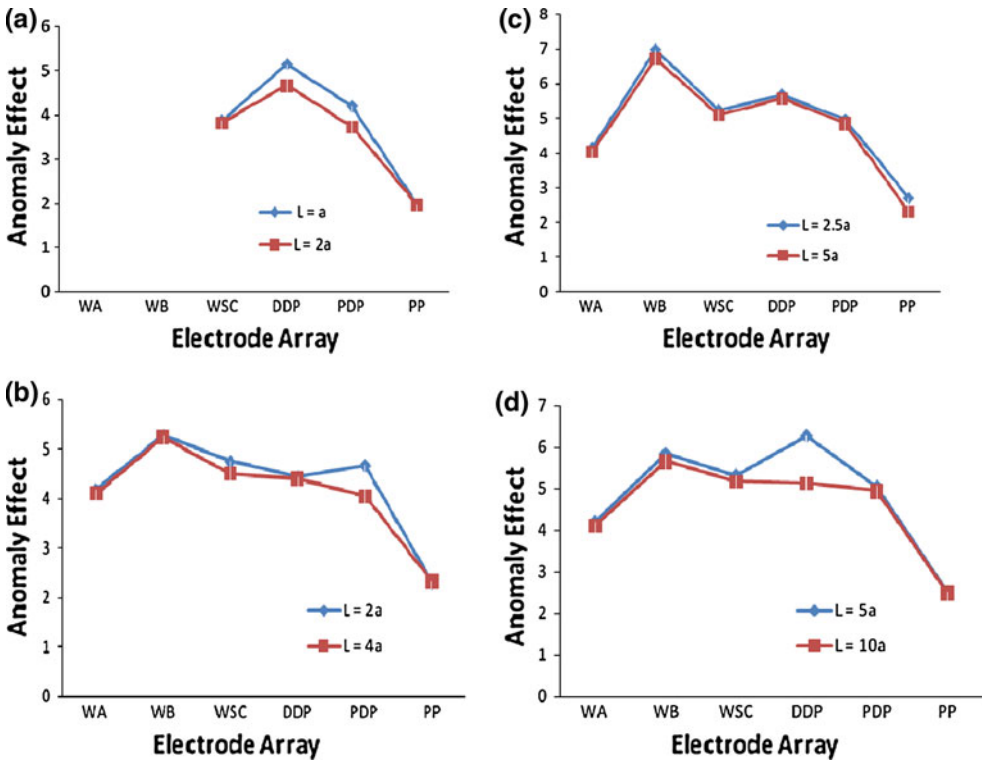

Fig. 4 Mean absolute anomaly effect of electrode arrays on the trough synthetic model. 3D geoelectrical resistivity imaging using orthogonal set of 2D profiles with grid size: **a** 11 × 11, **b** 21 × 21, **c** 26 × 26 ($L = 5a$) and 31 × 31 ($L = 2.5a$), and **d** 51 × 51; L is inter-line spacing and a is the minimum electrode separation

These anomaly effects, when compared with those shown in Figs. 3 and 4, show that the anomaly effects of electrode configurations on subsurface structures in 3D geoelectrical resistivity imaging surveys can be significantly improved by collating orthogonal sets of 2D apparent resistivity data measured with two different arrays in perpendicular directions. This indicates that the good quality and high-resolution 3D model images can be produced by inverting the 3D data set collated from 2D profiles of orthogonal paired-arrays. Thus, the efficiency and effectiveness of 3D geoelectrical resistivity imaging can be enhanced by measuring series of 2D apparent resistivity field data using two different electrode arrays in perpendicular directions such that data in parallel 2D profiles are observed by one array type and those in a perpendicular direction by another array type.

In Fig. 5, DDP–PDP, DDP–PP, DDP–WSC and PDP–PP orthogonal paired-arrays generally produce higher anomaly effects on the horst model whereas DDP–WB and WA-WSC orthogonal paired-arrays yield the lowest anomaly effects on the same model. Similarly, DDP–PDP, DDP–WB, PDP–WB and WB–WSC paired-arrays give higher anomaly effects while PDP–PP and PP-WA paired-arrays give the least anomaly effects on the trough model. The observed anomaly effects indicate that DDP–PDP, DDP–PP, DDP–WSC, PDP–PP, DDP–WB, PDP–WB and WB–WSC orthogonal paired-arrays are more sensitive to 3D features than the other orthogonal paired-arrays investigated. Thus, these orthogonal paired-arrays with better anomaly effects could be used to measure an orthogonal set of 2D apparent resistivity data that would be collated to a 3D data set such that the 2D profiles in a parallel direction are measured with a particular electrode array type and the 2D profiles in perpendicular direction are measured with the second electrode array in the orthogonal pair. The 3D resistivity images (inversion models or pseudosections) that would be obtained using such a technique would contain features of both arrays in the orthogonal pair used for the apparent resistivity measurements.

The anomaly effects of electrode arrays on the synthetic models for conventional 3D surveys in which 3D apparent resistivity measurements are made with square or rectangular grids of electrodes were also determined and are given in Fig. 6. There are no observable significant differences between the anomaly effects on the synthetic models presented in Fig. 6 and the anomaly effects on the synthetic models for the 3D data sets generated by collating orthogonal sets of 2D profiles shown in Figs. 3, 4 and 5. This suggests that collating a data set from a net of orthogonal 2D profiles, either of the same array type or orthogonal paired-array, to a 3D data set is effective for 3D geoelectrical resistivity survey.

The observed anomaly effect of the arrays on the synthetic models largely depends on the electrode grid size (or minimum electrode separation) and data density. The

anomaly effect on the synthetic models generally increases with increasing data density which depends on the minimum electrode separation a and data level n used in the computation of the apparent resistivity data as well as the electrode grid size and inter-line spacing L between the 2D lines. The anomaly effects shown in Figs. 3, 4 and 5 are compared with the electrode grid size and inter-line spacing L relative to the minimum electrode separation. The dependence of the anomaly effect of array on the inter-line spacing relative to the minimum electrode separation used in the determination of the apparent resistivity values could not be definitely established. However, the results indicate that the anomaly effect of electrode arrays on the synthetic models increases with decreasing inter-line spacing. We suggest that inter-line spacing equals or less than $4a$, where a is the minimum electrode separation, would yield high resolution and good quality model inversion images. 3D data sets with inter-line spacing slightly greater than $4a$ can still yield model inversion images with reasonable and acceptable resolution; but the model inversion images would contain more near-surface artefacts capable of distorting the interpretation.

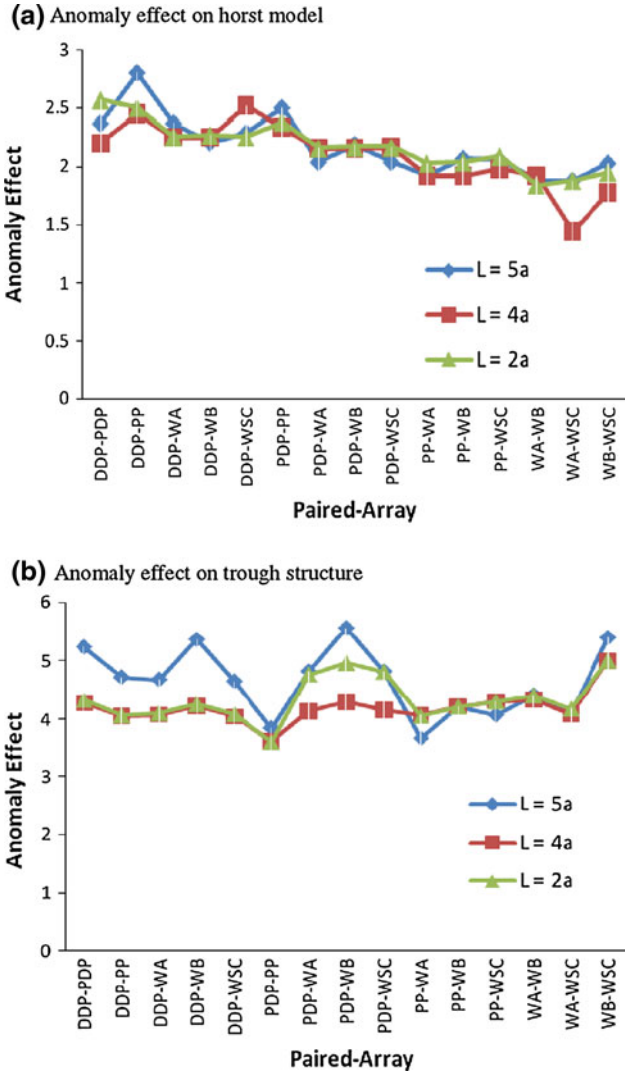

Fig. 5 Mean absolute anomaly effects of paired-arrays on: **a** horst and **b** trough models. Orthogonal set of 2D profiles in which all parallel 2D profiles are observed with one electrode array type and those in a perpendicular direction are observed with a different array

Conclusions

The observed anomaly effects of electrode configuration on the synthetic geological models show that collating orthogonal sets of 2D apparent resistivity data to a 3D data set is an effective and efficient technique for 3D geoelectrical resistivity surveys. If apparent resistivity data of 2D profiles are collated to 3D data sets such that profiles in a parallel direction are obtained using a particular array type and those in a perpendicular direction are observed by a different array, the relative efficiency and effectiveness of the arrays can be harnessed. DDP–PDP, DDP–PP, DDP–WSC, PDP–PP, DDP–WB, PDP–WB and WB–WSC orthogonal paired-arrays, which were found to be more sensitive to 3D features than the other orthogonal arrays investigated, are particularly recommended for 3D geoelectrical resistivity surveys in which the 3D data sets are collated from 2D apparent resistivity data using orthogonal paired-arrays. The observed anomaly effects on the

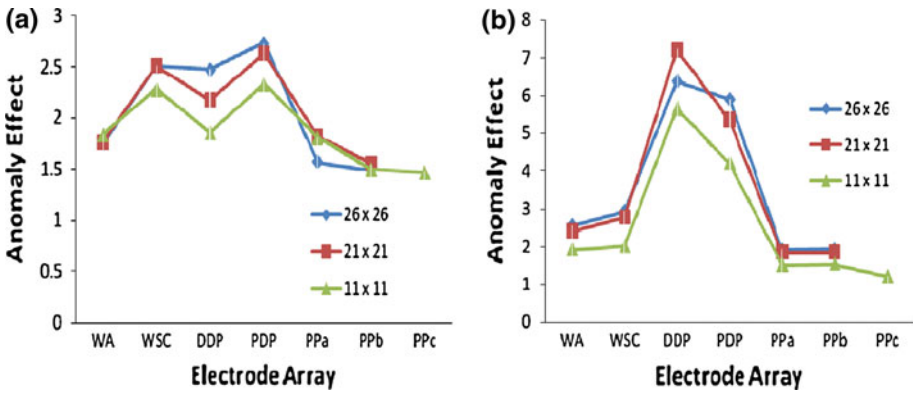

Fig. 6 Mean absolute anomaly effects of electrode arrays on: **a** horst and **b** trough models. Conventional 3D resistivity imaging using square or rectangular grids of electrodes (PPa correspond to PP used in Figs. 3, 4, 5). *PPa* pole–pole (in-lines), *PPb* pole–pole (cross-diagonal), *PPc* pole–pole (complete data set measured in all possible directions)

synthetic models for the orthogonal paired-arrays are independent of the electrode parameters and data density. No significant difference was observed between these anomaly effects of the orthogonal paired-array and the anomaly effect of the conventional square or rectangular grid of electrodes. This indicates that the use of 2D profiles of orthogonal paired-arrays for 3D geoelectrical resistivity survey is effective. The use of orthogonal paired-array in 3D geoelectrical resistivity surveys could be very useful to applications involving hydrogeological, environmental and engineering investigations, where the subsurface is usually highly heterogeneous.

References

Aizebeokhai AP, Olayinka AI, Singh VS (2009) Numerical evaluation of 3D geoelectrical resistivity imaging for environmental and engineering investigations using orthogonal 2D profiles. SEG Expanded Abstracts 28:1440–1444. doi:10.1190/1.3255120

Aizebeokhai AP, Olayinka AI, Singh VS (2010) Application of 2D and 3D geoelectrical resistivity imaging for engineering site investigation in a crystalline basement terrain, southwestern Nigeria. J Environ Earth Sci. doi:10.1007/s12665-010-0474-z

Amidu SA, Olayinka AI (2006) Environmental assessment of sewage disposal systems using 2D electrical resistivity imaging and geochemical analysis: a case study from Ibadan, Southwestern Nigeria. Environ Eng Geosci 7(3):261–272

Bentley LR, Gharibi M (2004) Two- and three-dimensional electrical resistivity imaging at a heterogeneous site. Geophysics 69(3): 674–680

Carruthers RM, Smith IF (1992) Hydrogeology of crystalline basement aquifers in Africa. In: Wright EP, Burgess WG (eds) The use of ground electrical survey methods for sitting water supply boreholes in shallow crystalline basement terrain. Geological Society Special Publication 66, pp 203–220

Chambers JE, Ogilvy RD, Meldrum PI, Nissen J (1999) 3D electrical resistivity imaging of buried oil-tar contaminated waste deposits. Eur J Environ Eng Geophys 4:3–15

Chambers JE, Ogilvy RD, Kuras O, Cripps JC, Meldrum PI (2002) 3D electrical mapping of known targets at controlled environmental test site. Environ Geol 41:690–704

Dahlin T, Loke MH (1998) Resolution of 2D Wenner resistivity imaging as assessed by numerical modelling. J Appl Geophys 38(4):237–248

Dahlin T, Zhou B (2004) A numerical comparison of 2D resistivity imaging with 10 electrodes array. Geophys Prospect 52:379–398

Dey A, Morrison HF (1979) Resistivity modelling for arbitrary shaped two-dimensional structures. Geophys Prospect 27:1020–1036

Griffiths DH, Barker RD (1993) Two dimensional resistivity imaging and modelling in areas of complex geology. J Appl Geophys 29:211–226

Griffiths DH, Turnbull J, Olayinka AI (1990) Two-dimensional resistivity mapping with a complex controlled array. First Break 8(4):121–129

Hazell JRT, Cratchley CR, Jones CRC (1992) The hydrology of crystalline aquifers in northern Nigeria and geophysical techniques used in their exploration. In: Wright EP, Burgess WG (eds) Hydrogeology of crystalline basement aquifers in Africa. Geological Society Special Publication 66, pp 155–182

Koefoed O (1979) Geosounding principles. 1. Resistivity sounding measurements. Elsevier, Amsterdam

Li Y, Oldenburg DW (1994) Inversion of 3D DC resistivity data using an approximate inverse mapping. Geophys J Int 116:527–537

Loke MH, Barker RD (1996) Practical techniques for 3D resistivity surveys and data inversion. Geophys Prospect 44:499–524

Militzer H, Rosler R, Losch W (1979) Theoretical and experimental investigations of cavity research with geoelectrical resistivity methods. Geophys Prospect 27:640–652

Ogilvy R, Meldrum P, Chambers J (1999) Imaging of industrial waste deposits and buried quarry geometry by 3D tomography. Eur J Environ Eng Geophys 3:103–113

Olayinka AI (1999) Advantage of two-dimensional geoelectrical imaging for groundwater prospecting: case study from Ira, southwestern Nigeria. J Natl Assoc Hydrogeol 10:55–61

Olayinka AI, Yaramanci U (1999) Choice of the best model in 2-D geoelectrical imaging: case study from a waste dump site. Eur J Environ Eng Geophys 3:221–244

Park S (1998) Fluid migration in the vadose zone from 3D inversion of resistivity monitoring data. Geophysics 63:41–51

Press WH, Teukolsky SA, Vetterling WT, Flannery BP (1996) Numerical recipes in Fortran 77: the art of scientific computing, 2nd edn. Cambridge University Press, Cambridge

Telford WM, Geldart LP, Sheriff RE, Keys DA (1976) Applied geophysics. Cambridge University Press, London, p 860